Thin-Film Fluid Flows over Microdecorated Surfaces: Observation of Polygonal Hydraulic Jumps

Emilie Dressaire,[1] Laurent Courbin,[1,2] Jérome Crest,[1] and Howard A. Stone[1,*]

[1]School of Engineering and Applied Sciences, Harvard University, Cambridge, Massachusetts 02138, USA
[2]IPR, UMR CNRS 6251, Campus Beaulieu, Université Rennes 1, 35042 Rennes, France

(Received 7 November 2008; published 15 May 2009)

Liquid films flowing over rough substrates are influenced by asperities whose sizes are comparable to the film thickness. We investigate flows driven by jet impact on a regular array of micron-size posts. We show that the topography modifies the size and the shape of the observed hydraulic jumps: in addition to circular jumps, we obtain a variety of stable polygonal shapes. We rationalize our results by considering a leakage flow through the texture and the free-surface flow above it, coupled by an effective slip boundary condition accounting for the symmetry of the texture. This model is in good agreement with our experiments and allows us to account for the interplay between flow properties and roughness parameters, which has applicability in many other thin-film configurations.

DOI: 10.1103/PhysRevLett.102.194503 PACS numbers: 47.15.gm, 47.20.Ky, 83.50.Lh

The flow of thin films of liquid on a substrate [1] is of importance for diverse phenomena such as industrial processes that rely on rapid motion to produce sheets of uniform thickness [2], ordinary biological features including tear films in the eye [3], and even geological events such as lava flows [4]. Some discussions of the influence of the substrate topographical features on the thin-film thickness exist in the literature, e.g., the destabilization of the originally leveled free-surface [5]. Despite the well-established effects of isolated features on viscously dominated thin-film flows [6], the collective influence of micron-scale asperities organized on a regularly patterned substrate has not yet been considered. For such surfaces, a variety of hydrodynamic effects have been studied both experimentally [7–9] and theoretically [10]; in the latter, the texture introduces a slip boundary condition dependent on geometrical surface features.

In the case of thin-film flows over rough surfaces, previous studies focus on two limiting cases: fluid layers that are much thicker [11] or thinner [6] than the characteristic length scales of the texture. Here, we investigate thin liquid films formed upon impact of a jet of water on micro-textured surfaces: film thickness and roughness amplitude are of the same order of magnitude.

When a jet of sufficiently high flow rate impinges upon a smooth substrate, the liquid sheet generated by impact is bounded by a circular abrupt rise of the surface, known as a hydraulic jump [12]. The jump is the visible signature of an abrupt velocity change [13–15]. We show that a regular, micron-scale surface topography can induce a symmetry breaking of the circular hydraulic jump: the shapes even exhibit sharp corners. We study experimentally this phenomenon and demonstrate that the polygonal structures are controlled by the geometry of the surface topography; the symmetry breaking is not a signature of viscous and inertial capillary instabilities [16,17]. We rationalize our observations by using a boundary-layer approach [13] to describe the flow in the thin film, above the posts. In our model, the presence of the texture reduces the flow rate in the thin film and introduces a slip boundary condition. We show below that this approach captures the main features of the polygonal jumps, both their shapes and mean radii.

Experiments.—Water is pumped into a nozzle of radius $a = 1.2$ mm at a controlled flow rate, $Q = 0.5$–$2.5\ \mathrm{L \cdot min^{-1}}$ [Fig. 1(a)]. The jet impacts the center of a patterned disc of PDMS of radius 2.5 cm, which is embedded in a smooth clear acrylic plate [Fig. 1(b)]. The patterned surface consists of square or hexagonal arrays of cylindrical posts with height H, radius R and lattice distance D of the order of 100 μm. The water spreads radially over the rough substrate, then over the smooth surrounding area, before spilling into the collection reservoir. The thickness $h(r)$ of the thin film propagating before the jump is of the order of a few hundreds of microns, whose value is estimated assuming flow rate conservation and a constant velocity ($h(r) \sim \frac{a^2}{r}$, with $r \approx 1$ cm). The depth of the water layer outside the jump is $d \approx 4.3$ mm. Our measurements show that d does not depend on the flow rate and the substrate topography. The radial position of the jump is measured for 200 evenly distributed angular positions, by analyzing the image with a custom-written MATLAB software.

A typical observation, obtained when a jet impacts a square lattice is shown in Fig. 1(c): the jump, which is located on the smooth substrate beyond the patterned disc, adopts an eight-corner star shape. The use of patterned substrates allows the formation of steady, stable polygonal shapes at the centimeter scale. To rationalize these observations, we study the roles of the lattice geometry and the fluid properties. Since the velocity in the layer beyond the jump is negligible compared to the velocity in the thin film, the characteristics of the flow in the outer layer are assumed constant here.

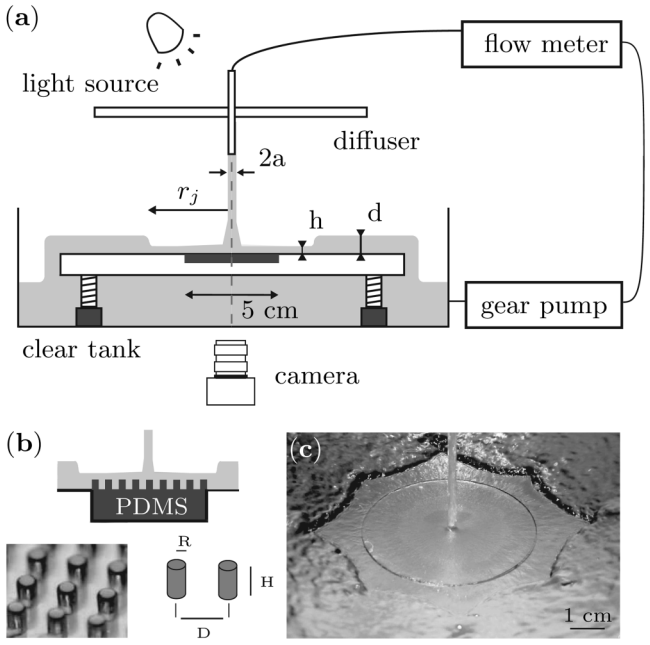

FIG. 1. Experimental method. (a) Schematic of the experimental setup. (b) The micropattern embedded in the center of the impact plate. The photograph shows the cylindrical posts of polydimethylsiloxane (PDMS) arranged on a square lattice. The typical radius R and height H of the posts and lattice distance D are approximately 100 μm. (c) Photograph of a polygonal jump taken from above, at a 45° angle. The jump is formed by a water jet ($Q = 1\ \mathrm{L \cdot min^{-1}}$) impacting a square lattice ($D = 200\ \mu$m, $R = 50\ \mu$m, and $H = 50\ \mu$m).

We begin by varying the symmetry of the lattice. Jumps of the same mean radius but formed over different micropatterned surfaces adopt a variety of reproducible polygonal shapes [Fig. 2]. When the jet impinges on hexagonal or square arrays, the jumps form hexagonal (b) and eight-corner shapes (c). In both cases, the lattice and jump symmetries are similar, respectively, sixfold and fourfold. The corners of the polygonal shapes are pointing toward the main lattice directions, e.g., along both the diagonals and the axes for the square arrays.

The robustness of the shape selection by the micropatterns is tested by modifying fluid properties such as kinematic viscosity $\nu = 1\text{–}3.5 \times 10^{-6}\ \mathrm{m^2 \cdot s^{-1}}$ and air/water surface tension, $\gamma = 30\text{–}70 \times 10^{-3}\ \mathrm{N \cdot m^{-1}}$ [18]. For a given mean radius, the jumps retain the same polygonal shapes. These observations show that the symmetry breaking is not induced by a viscocapillary or an inertiocapillary instability [16,17].

We next vary systematically the parameters of a square lattice, both the lattice distance D and the height of the posts H. The observations are reported in Fig. 3. The mean radius of the jump increases nonlinearly with the flow rate. The corners of the polygonal structures are sharper for larger flow rates. Indeed, at small flow rates, the polygonal structures can not be distinguished from fluctuations; the jumps therefore appear as nearly circular to the naked eye. The shape and the average radius of the jump are also influenced by the lattice properties: at a given flow rate, the corners of the polygons are sharper, and the mean radius smaller, for smaller lattice spacing and taller posts. Since in the classical theory for circular jumps [13] the radius increases monotonically with the flow rate, we interpret the decrease in mean radius observed in our experiments as indicative of the reduction of the average flow rate in the thin film above the posts: some of the liquid flows through the microtexture. The results reported in Fig. 3 show that

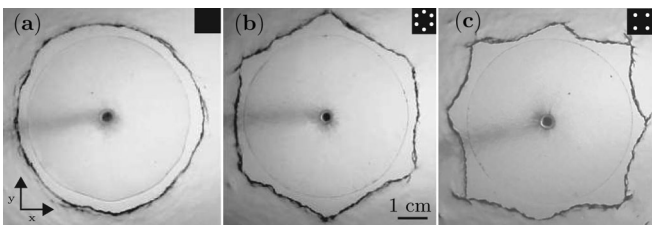

FIG. 2. Influence of pattern structure. Water jets impact (a) a smooth substrate ($Q = 1.3\ \mathrm{L \cdot min^{-1}}$), (b) a hexagonal lattice ($Q = 1.7\ \mathrm{L \cdot min^{-1}}$), and (c) a square lattice ($Q = 1.9\ \mathrm{L \cdot min^{-1}}$). Lattice parameters: $D = 200\ \mu$m, $R = 50\ \mu$m, and $H = 50\ \mu$m.

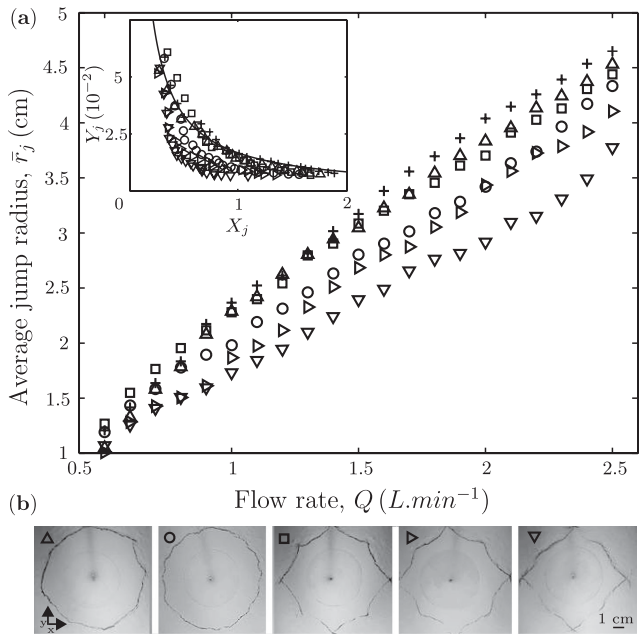

FIG. 3. Influence of pattern geometry on the jump. (a) Average radius versus flow rate for four square lattices with post radius $R = 50\ \mu$m and different lattice spacing and posts heights: (△) $D = 200\ \mu$m and $H = 23\ \mu$m, (▷) $D = 200\ \mu$m and $H = 50\ \mu$m, (▽) $D = 200\ \mu$m and $H = 88\ \mu$m, (○) $D = 300\ \mu$m and $H = 50\ \mu$m, (□) $D = 400\ \mu$m and $H = 50\ \mu$m. Inset, the data are compared to predictions (solid line) with $Y_j = \bar{r}_j g(\frac{da}{Q})^2(1 + \frac{2}{\bar{B}_0}) + \frac{a^2}{2\pi^2 \bar{r}_j d}$ and $X_j = \frac{\nu(\bar{r}_j^3 + \ell^3)}{Qa^2}$ [19], where $\bar{B}_0 = \frac{\rho g \bar{r}_j d}{\gamma}$ is the Bond number. (b) Images of the polygonal jumps over different substrates for $Q = 2.5\ \mathrm{L \cdot min^{-1}}$.

both the anisotropy and the average value of the jump radius depend on the flow rate, the height of the posts and the lattice spacing. We further illustrate the influence of the roughness on the jump by comparing the experimental data to previous predictions for a smooth substrate [19] [inset of Fig. 3(a)]. Only data corresponding to nearly circular jumps collapse onto the curve of an existing model for smooth substrates.

Discussion.—To better capture the role of the roughness, we note that the systematic reduction in jump radius can be rationalized by a reduced flow rate. The flow rate of the jet is divided into a ''leakage'' flow rate through the roughness and a thin-film flow above the posts. The flow is characterized by an intermediate Reynolds number upon impact ($\mathrm{Re} \sim \frac{QR}{\nu\pi a^2} \sim 250$). Because of friction in the microtexture, the fluid velocity through the posts decreases rapidly and the ''leakage'' flow reaches a low Reynolds number, associated with an isotropic permeability [20]. The complications of the detailed structure, which is bounded by the substrate at the bottom and a liquid film flowing at the top, lead us to approximate the leakage flow rate as radial and varying linearly with the total flow rate: $q_{\mathrm{leak}} = \alpha Q$ with α a nontrivial function of the roughness porosity ($\epsilon = 1 - \frac{\pi R^2}{D^2}$) and the aspect ratio of the posts ($\kappa = \frac{H}{R}$), i.e., a measurement of the isotropic permeability of the shallow porous layer. Therefore, the thin film flowing above the posts has a reduced flow rate, $(1 - \alpha)Q$.

The free-surface flow can be studied following a classical approach [13], where the inertia-dominated radial motion has a boundary-layer structure, which grows from the stagnation point, until it totally invades the thin film. The roughness introduces a slip boundary condition at the top of the posts ($z = 0$) where the radial velocity u satisfies a Navier boundary condition: $u = \lambda \frac{\partial u}{\partial z}$. The structure of the slip length is prescribed by the boundary-layer approach: for a similarity solution to exist, as in [13], we write $\lambda = bh(r)$, with $h(r)$ the thickness of the fluid film above the posts. In the spirit of high Reynolds number flow phenomena consistent with the intermediate Reynolds number regime considered here, which is not yet explored to the best of our knowledge, the slip length is expected to have the same anisotropy as the lattice. Thus the nondimensional parameter b is defined by the following constitutive relation $b(\theta, \xi) = \xi \frac{\ell_0(\theta)}{2D}$, where $\xi(\epsilon, \kappa)$ is a function of the roughness porosity and the aspect ratio of the posts,

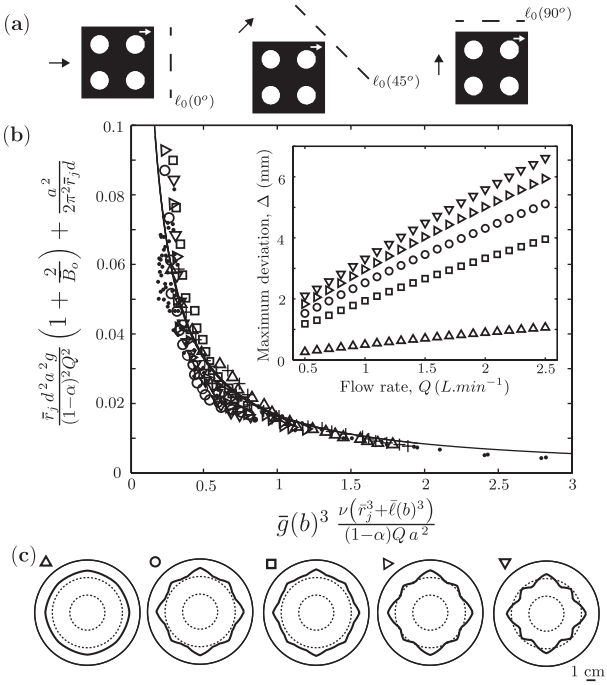

FIG. 4. Results of the modeling. (a) View from above of a unit cell of a square lattice. Black and white arrows indicate, respectively, the flow direction and the main axis of the lattice. θ is the angle between these two directions (here, 0°, 45°, and 90°) and ℓ_0, which scales as the open frontal area, is represented by the black lines. (b) Comparison between the results of the model (solid line) and the experimental data. The results obtained in [15] are also represented (•). $\bar{\ell}(b)$, $\bar{g}(b)$, $\bar{B}_0$, and $\bar{r}_j$ are averaged for θ between 0 and 2π. Inset: Maximum deformation of the shape as predicted by the model. (c) Shapes predicted square lattices with different lattice parameters. Symbols are as in Fig. 3.

whose value is determined experimentally. Here $\ell_0(\theta)$ determines the angular variation of the slip length: phenomenologically, we find that this dependence is well captured by the open frontal area, which corresponds to the width of the channels delimited by rows of posts as illustrated in Fig. 4(a).

The reduced flow rate in the film and the slip boundary condition defined above are accounted for in a boundary-layer approach, which considers the flow as unidirectional for each value of the angle θ and so determines a jump radius, $r_j(\theta)$. This approach leads to a modified definition of the position of the jump that depends on α and $b(\theta, \xi)$:

$$r_j(\theta) g\left(\frac{da}{(1-\alpha)Q}\right)^2\left(1+\frac{2}{B_0}\right)+\frac{a^2}{2\pi^2 r_j(\theta) d}=\frac{27\sqrt{3}}{8\pi^6}\left(\frac{c}{g(b)}\right)^3 \frac{(1-\alpha)Qa^2}{\nu(r_j(\theta)^3+\ell(b)^3)}. \quad (1)$$

For a given value of θ, the position of the jump r_j is obtained by balancing the momentum across the jump [19]. The first term corresponds to the gravitational body force and the surface tension contribution with the Bond number $B_0 = \frac{\rho g r_j d}{\gamma}$. The other terms represent inertial effects and c is a numerical constant; see [13,15]. The slip boundary condition modifies the velocity inside the jump through two analytical functions $g(b)$ and $\ell(b)$ [19].

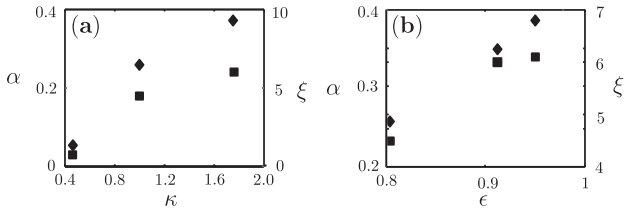

FIG. 5. Coefficients of the model. Leakage flow (α, ◆) and slip length (ξ, ■) coefficients as functions of: (a) The aspect ratio of the posts κ, for a fixed value of the roughness porosity ϵ (H varies, R and D are constant); (b) ϵ, for a fixed value of κ (D varies, R and H are constant).

For each lattice structure the two unknown parameters α and ξ are determined by matching the values of the jump mean radius obtained experimentally and predicted by Eq. (1) for the highest flow rate, $Q = 2.5\ \mathrm{L} \cdot \mathrm{min}^{-1}$. We then compare the predictions of the model to the experimental observations, with a given value α and ξ now associated to each lattice geometry. In Fig. 4(b), we compare the evolution of the mean radius of the jump with the flow rate of the jet, using a representation similar to the one adopted in the inset of Fig. 3(a); the experimental points collapse on the model curve defined by Eq. (1).

The model also predicts the value of the amplitude of the jump deformation, $\Delta = \max(r_j) - \bar{r}_j$ [inset of Fig. 4(b)]. The deformation increases with the flow rate, which is consistent with our experimental observations: at low flow rate, the shapes appear circular because the deformation is too small to be distinguished from fluctuations. Figure 4(c) shows the shapes of the jumps predicted by Eq. (1), for the different lattice geometries. As presented in this figure, the model captures the main features of our experimental observations.

Finally, we provide the values of α (leakage through the porosity) and ξ (magnitude of slip) determined by fitting the experimental data (Fig. 5): both α and ξ are increasing functions of the porosity of the roughness and the aspect ratio of the posts. We note that the evolution of the slip prefactor ξ is monotonic in the parameters, which is consistent with the dependence reported recently for flow over a porous layer at low Reynolds number [21].

Conclusion.—We report that regularly micropatterned substrates can modify the position and the shape of the hydraulic jump: we observe a smooth transition from the familiar circular shape to polygonal structures. We rationalize our observations by considering a leakage flow through the porosity and a free-surface flow above the posts. The properties of the two fluid layers are coupled through mass conservation and the slip boundary condition at the top of the posts. This study illustrates that a regular roughness can strongly disturb the velocity field in a thin liquid film, effects that could be exploited to control the properties of liquid sheets.

The authors thank A. Ajdari, M. Bazant, T. Bohr, J. Bush, and C. Clanet for helpful conversations. We also thank the Harvard MRSEC (DMR-0820484) and Schlumberger for support of this research.

*has@seas.harvard.edu

[1] For a review, see for instance A. Oron, S. H. Davis, and S. G. Bankoff, Rev. Mod. Phys. **69**, 931 (1997).
[2] *Modern Coating and Drying Technology*, edited by E. D. Cohen and E. B. Gutoff (Wiley, Hoboken, 1992).
[3] A. Sharma and E. Ruckenstein, J. Colloid Interface Sci. **113**, 456 (1986).
[4] H. E. Huppert and J. E. Simpson, J. Fluid Mech. **99**, 785 (1980).
[5] L. M. Peurrung and D. B. Graves, J. Electrochem. Soc. **138**, 2115 (1991).
[6] S. Kalliadasis and G. M. Homsy, J. Fluid Mech. **448**, 387 (2001).
[7] J. Bico, U. Thiele, and D. Quéré, Colloids Surf. A **206**, 41 (2002).
[8] L. Courbin, E. Denieul, E. Dressaire, M. Roper, A. Ajdari, and H. A. Stone, Nature Mater. **6**, 661 (2007).
[9] C. Pirat, M. Sbragaglia, A. M. Peters, B. M. Borkent, R. G. H. Lammertink, M. Wessling, and D. Lohse, Europhys. Lett. **81**, 66 002 (2008).
[10] M. Z. Bazant and O. I. Vinogradova, J. Fluid Mech. **613**, 125 (2008).
[11] A. M. J. Davis and D. F. James, Transp. Porous Media **53**, 175 (2003).
[12] Lord Rayleigh, Proc. R. Soc. A **90**, 324 (1914).
[13] E. J. Watson, J. Fluid Mech. **20**, 481 (1964).
[14] T. Bohr, V. Putkaradze, and S. Watanabe, Phys. Rev. Lett. **79**, 1038 (1997).
[15] J. W. M. Bush and J. M. Aristoff, J. Fluid Mech. **489**, 229 (2003).
[16] C. Ellegaard, A. E. Hansen, A. Haaning, K. Hansen, A. Marcussen, T. Bohr, J. L. Hansen, and S. Watanabe, Nature (London) **392**, 767 (1998); Nonlinearity **12**, 1 (1999).
[17] J. W. M. Bush, J. M. Aristoff, and A. E. Hosoi, J. Fluid Mech. **558**, 33 (2006).
[18] E. Dressaire, L. Courbin, J. Crest, and H. A. Stone (to be published).
[19] See EPAPS Document No. E-PRLTAO-102-050922 for a more detailed presentation of the model. For more information on EPAPS, see http://www.aip.org/pubservs/epaps.html.
[20] D. L. Koch and A. J. C. Ladd, J. Fluid Mech. **349**, 31 (1997).
[21] U. Thiele, B. Goyeau, and M. G. Velarde, Phys. Fluids **21**, 014103 (2009).